

A DUAL-ANTENNA MOBILE ROBOT ORIENTATION ESTIMATION SYSTEM BASED ON RSSI FINGERPRINTING AND MACHINE LEARNING TECHNIQUES

Mateusz SUMOREK^{*}, Adam IDŹKOWSKI^{*}

^{*}Faculty of Electrical Engineering, Institute of Automation, Electronic and Electrical Engineering, Bialystok University of Technology, Wiejska st. 45D, PL-15351 Bialystok, Poland

mateusz.sumorek@pb.edu.pl, a.idzkowski@pb.edu.pl

received 01 August 2025, revised 09 November 2025, accepted 09 November 2025

Abstract: This paper introduces a switchable, dual-antenna Wi-Fi tracker that is based on an ESP32-ROOM-DA chip and a BNO085 IMU. The tracker is intended to estimate object orientation in confined spaces by utilizing fingerprinting techniques and differences in RSSI values. The research aimed to provide an alternative that does not necessitate magnetometer calibration or intricate antenna arrays, thereby eliminating the constraints associated with expensive AoA systems and magnetometers that are susceptible to interference. Experiments were conducted in a 5 x 5 m test area of a sports hall, with seven randomly distributed access points (APs) within the sports hall. Five APs were in the LOS (line of sight) zone, and two others, which were available in the building, were in the NLOS (non-line-of-sight) zone. The measurements were performed by a DJI Robomaster S1 robot, which was equipped with the tracker. Training data were collected at 100 points; 14 randomly selected locations were used for testing, with eight distinct orientations for every measurement point. During the measurement, the RSSI from both antennas of individual APs, as well as their SSIDs, was recorded. Additionally, the IMU quaternions were mapped to the cardinal directions (N, W, S, E). Four classifiers were trained using the features gathered: k-NN, SVM, Random Forest, and MLP. The k-NN classifier achieved the best performance (MCC 0.23, F1 score 0.39). The dual-antenna system can distinguish the cardinal directions, as evidenced by the results. However, it is imperative to balance the training dataset and collect a greater number of samples to reduce the effect of multipath and NLOS conditions. With more research, it is possible to use an expanded multi-antenna system and the newest Wi-Fi standards. Furthermore, modifications to the measurement process are planned to guarantee a balanced training set.

Key words: indoor localization, orientation estimation, RSSI, fingerprinting, antenna, mobile robot

1. INTRODUCTION

Indoor location is a fundamental element of modern systems for intelligent buildings and enterprises, robotics, and the Internet of Things (IoT). There is a significant amount of interest in this subject, as evidenced by the number of publications that have been published in recent years [1,2].

Satellite navigation systems, including GPS, GLONASS, Galileo, and BeiDou, do not apply to indoor location, despite their high accuracy in open spaces. This is primarily an effect of the limited propagation of radio signals through building structures, which effectively prevents location or significantly reduces its accuracy [3].

Due to their ubiquity, relatively low implementation costs, and the ability to adapt existing infrastructure, radio technologies are very popular in indoor environments. Examples of such technologies include Bluetooth, Wi-Fi, RFID, and UWB (Ultra-Wide Band) [3–7]. Although the accuracy of such solutions is still limited, continuous research and standards development are being conducted to make the solutions more usable.

The majority of indoor location systems focus on determining the position of an object in two- or three-dimensional space. Frequently, the orientation (angular position) of the object relative to a fixed reference frame is crucial information in addition to its position. This enables the determination of the object's pose in a 6-degree-of-freedom space. This is important in the context of industrial

asset management systems, indoor navigation systems, and autonomous robots [8].

Commonly, magnetometers are used as compasses to find the orientation of an object. This facilitates the determination of the object's orientation in relation to the magnetic poles of the Earth. There are a lot of sources of soft iron and hard iron interference in the industrial environment, so this solution might not work there [9,10]. Additionally, these solutions necessitate periodic calibration [10].

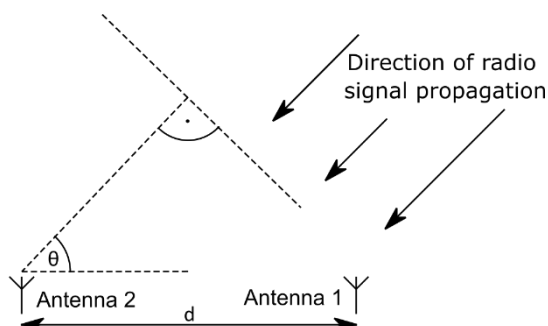


Fig. 1. Graphical representation of the angle of arrival

The Angle of Arrival (AoA) technique is one of the radio techniques used to determine orientation. It is a component of the Bluetooth standard called Direction Finding [11]. This solution is based

on the utilization of antenna arrays and the measurement of the phase difference of the received signal between individual antennas of the array, the distance between which is already known (Figure 1). This solution is susceptible to multipath phenomena, has a high technological cost, and is subject to limitations in accuracy under NLOS (Non-Line of Sight) conditions [12]. An alternative approach is the utilization of optical detectors, which enable the simultaneous precise positioning at 6.55 cm and orientation with an accuracy of 0.51° [13]. However, this solution necessitates a specialized infrastructure and is restricted to operation in Line of Sight (LOS) conditions. In addition, the literature provides angle of arrival estimations that are derived from RSSI (Received Signal Strength Indicator) measurements and a rotating antenna system. Finding signal minima in the spatial characteristics of the antennas is the foundation of the estimation process. The results showed that the mean absolute error was 4° when the test was done outside and 6° when it was done inside a building [14]. This solution necessitates a distinct mechanical structure and employs numerous radio receivers that must communicate with one another to process data from each one.

This article discusses the proposed solution, which is a switchable dual-antenna system that estimates orientation using machine learning fingerprinting techniques and RSSI value differences.

Cardinal directions (north, south, east, and west) were classified based on compass readings. The classification process employed the k-NN (k-Nearest Neighbors), SVM (Support Vector Machines), Random Forest (RNF), and Multi-Layer Perceptron (MLP) models. Sensitivity, precision, F1-score, and Matthews Correlation Coefficient (MCC) were determined to evaluate the quality of the models.

In contrast to a multi-receiver system, the device design is simplified by the use of a switchable dual-antenna system. In comparison to a single-antenna system, it is feasible to acquire additional information by exploiting the anisotropy of the antennas' directional characteristics. This translates to the capacity to ascertain the direction, analogous to the AoA method [14, 15].

The subsequent sections of the article are structured as follows: Section 2 discusses the technical aspects of the approach and the methodology required to comprehend the work. Section 3 describes the process of evaluating the quality of the developed methods and their underlying principles. In Section 4, the results and an analysis of them for each model are shown. The conclusions are presented in Section 5.

2. PROPOSED METHOD

2.1. Site selection

The experiment was conducted in the sports hall of the Bialystok University of Technology. Access points (APs) were randomly placed within the hall as shown in Figure 2. A total of seven access points were set up, two of which were located in the NLOS area. Four access points in the LOS zone were placed at a height of 2.5 m, one at height of the 0.7 m (on the table). Access points installed in the building were also used.

A picture of the experiment can be found in Figure 3. It illustrates the APs located in the LOS zone, the control station from which the entire experiment was managed, and the robot on which the tracker was mounted. One of the APs in the NLOS zone is depicted in Figure 4.

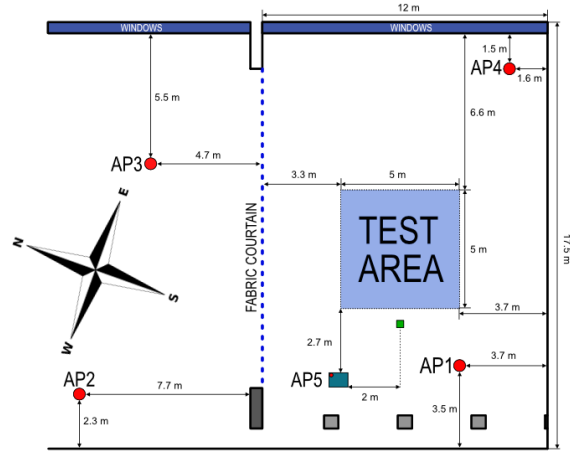


Fig. 2. Equipment layout in the building

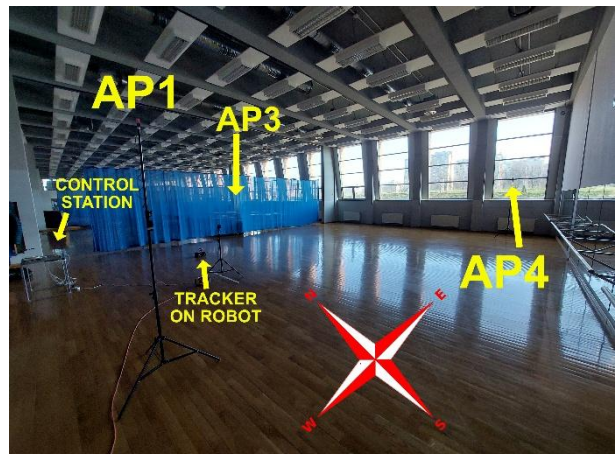


Fig. 3. Equipment layout in 3D view



Fig. 4. Wi-Fi router placed in the NLOS zone

2.2. Hardware configuration

RSSI measurements were conducted with a proprietary tracker (Figure 5). It contained an ESP32-WROOM-DA chip that enabled Wi-Fi and Bluetooth connectivity [16]. As illustrated in Figure 6, this chip features an antenna array that comprises two antennas that can alternately function through an integrated RF (Radio Frequency) switch. The antennas are positioned at a 90-degree angle

relative to each other. The device was also equipped with a BNO085 inertial measurement unit (IMU) with a 3-axis accelerometer, gyroscope, and magnetometer [17]. Furthermore, the chip was equipped with LEDs to indicate the operating status and a micro SD card slot, which enabled the storage of measurements on a memory card.

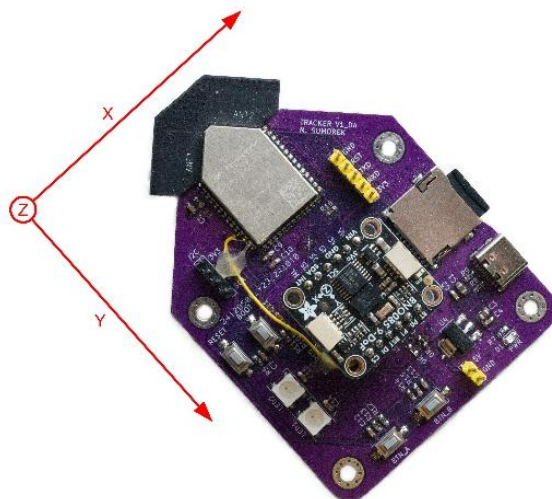


Fig. 5. The tracker with the IMU orientation marked

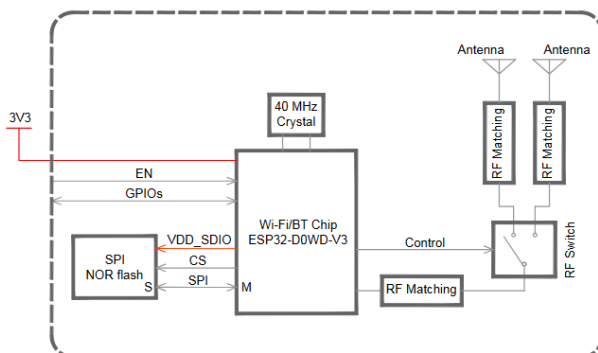


Fig. 6. The internal structure of the ESP32-WROOM-DA system [16]

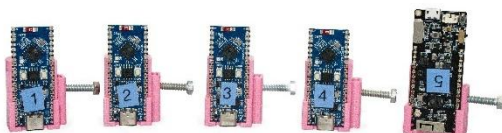


Fig. 7. ESP32 units used as APs

The access points (APs) used were ESP32 devices and two TP-Link Wi-Fi routers. The ESP32 devices are shown in Figure 7. They were mounted on tripods. The test devices operated under the IEEE 802.11 b/g/n Wi-Fi standards.

A DJI Robomaster S1 mobile robot was used for the tests (Figure 8). A tracker was placed on the robot. This allowed for the automation of the measurement process and the most faithful representation of the system's actual operating conditions. The robot's dimensions are 320 x 240 x 270 mm [18].



Fig. 8. Robomaster S1 robot with tracker mounted

2.3. Measurements and data

The data was collected in two sets by taking the measurements twice. To obtain training data, one set of data was gathered, and to obtain test data, another. The measurements were performed under static conditions – the robot did not move during the measurements.

The following data was collected during the measurements and subsequently utilized to train the models:

- a quaternion that shows the orientation in relation to the four cardinal directions from the BNO085 sensor,
- the RSSI values for individual access points from each antenna, as well as the SSID (Service Set Identifier) and the antenna designation from which the measurement was collected.

This data was saved in .csv format.

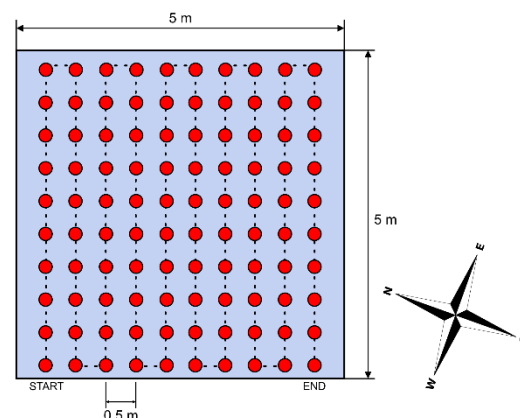


Fig. 9. The measurement route of the training set with marked measurement locations

The training set was measured using a grid of 0.5 m spacing in a square measuring approximately 5 x 5 m (Figure 9). A total of 100 points were measured. Each point was measured eight times. Each measurement was performed with the robot in a different orientation, i.e., rotating approximately 45° around the Z axis. This resulted in approximately 10,000 unique raw data records. Test data was acquired by taking measurements at 14 randomly distributed locations within the test area (Figure 2). Eight measurements were taken at each location, with the mobile robot rotating between each.

Tab. 1. Quaternion mappings [17]

BNO08X physical axis aligned			Mapping quaternion			
X	Y	Z	Qw	Qx	Qy	Qz
East	North	Up	1	0	0	0
North	West	Up	($\sqrt{2}/2$)	0	0	($\sqrt{2}/2$)
West	South	Up	0	0	0	1
South	East	Up	($\sqrt{2}/2$)	0	0	($-\sqrt{2}/2$)

According to Table 1 from the IMU manufacturer's documentation, the orientation expressed as a quaternion was mapped to the cardinal directions. These directions served as classification classes.

The data was preprocessed to remove erroneous measurements, particularly those with incorrect SSID encoding, which frequently occurred when the RSSI was less than -80 dBm. Outliers (measurements with extremely inaccurate RSSI values) were also removed. Measurements with the RSSI of 0 dBm were partially removed, suggesting that the antenna was unable to find the access point during that measurement.

After removing the majority of erroneous records from the datasets, they were grouped. The process of grouping involved combining measurements from the same pose into a single record, which reduced data about RSSI values from various APs to a single record. Both data processing stages resulted in a reduction of the training set to 736 records and the test set to 111 records. This corresponded to the number of poses in which measurements were taken (800 for the training set and 112 for the test set), excluding erroneous measurements.

Subsequently, the datasets were substantially expanded to incorporate variations in RSSI values between antennas and individual APs. Furthermore, the sets were supplemented with information regarding their position in relation to magnetic directions was also added. This information was used for classification. Four orientation classes were obtained as a result of the quaternion mapping process, as outlined in Table 1.

Tab. 2. Number of classes in the training set and their percentage share in the set

West	East	North	South
256	199	184	97
34,8%	27,0%	25,0%	13,2%

The distribution of class sizes in the training set is presented in Table 2. The unbalanced nature of the analyzed set is a critical factor in the assessment of model quality [19].

Tab. 3. Number of classes in the test set and their percentage share in the set

West	East	North	South
39	28	29	15
35,1%	25,2%	26,1%	13,5%

The distribution of class frequencies in the test set is presented in Table 3. The percentages are about the same as they were in the training set.

Despite the standardized data collection process, discrepancies in class size may be attributable, among other factors, to the mobile robot's wheel slippage on the surface it was traversing. This contributed to the discrepancy between the specified rotation and the actual change in orientation.

The data were normalized before the training process.

3. MODEL EVALUATION

The classification models were characterized by metrics in order to assess the results obtained using the developed models. Metrics such as precision, sensitivity, and F1 score were calculated. The analyzed problem is multi-class, and in addition to metrics for individual classes, micro- and macro-averages were also calculated [19–22].

The precision of a given class C is expressed by formula (1), it defines the ratio of correctly classified TP observations to all observations classified as class C, both correctly and incorrectly [20].

$$Precision_C = \frac{TP_C}{TP_C + FP_C} \quad (1)$$

where: TP_C – number of observations correctly classified into class C, FP_C – number of observations incorrectly classified as class C.

The micro-average precision expressed by equation (2) is the ratio of the sum of all (in each class) observations correctly classified to the sum of all (in each class) observations classified to a given class [20]. Since the sums refer to all classes, ultimately, it is the ratio of all values correctly classified to all classifications.

$$Precision_{micro} = \frac{\sum_{k=1}^K TP_k}{\sum_{k=1}^K (TP_k + FP_k)} = \frac{\sum_{k=1}^K TP_k}{Grand\ Total} \quad (2)$$

The macro-average precision expressed by the relation (3) is the average of the precision of individual classes [20].

$$Precision_{macro} = \frac{1}{K} \sum_{k=1}^K Precision_k \quad (3)$$

The sensitivity of class C described by equation (4) defines the ratio of correct classifications to the sum of all classifications classified into class C [20]. It measures what fraction of true positive TP observations was detected.

$$Recall_C = \frac{TP_C}{TP_C + FN_C} \quad (4)$$

where: TP_C – number of observations correctly classified into class C, FN_C – number of observations belonging to class C but classified incorrectly.

Analogously to micro-average precision, micro-average sensitivity is expressed as the ratio of the sum of all (in each class) observations correctly classified to the sum of all (in each class) classifications classified into a given class. Therefore, the value of micro-average sensitivity and precision are given the same value (5) [20].

$$Recall_{micro} = Precision_{micro} \quad (5)$$

The macro-average sensitivity expressed by equation (6) is the average sensitivity of each class [20].

$$Recall_{macro} = \frac{1}{K} \sum_{k=1}^K Recall_k \quad (6)$$

The F_1 score (7) is a metric that represents the harmonic mean of precision and sensitivity [20]. It can therefore be expressed for each class, as well as for the micro- and macro-average. This metric provides a compromise between precision and sensitivity, especially in cases where both metrics have extreme values. To obtain a high score, both metrics must be high. The F_1 score ranges from 0 to 1, where 0 indicates poor model performance and 1 indicates an ideal model.

$$F_1 = \frac{2}{\frac{1}{Precision} + \frac{1}{Recall}} \quad (7)$$

Because precision, sensitivity, and F_1 scores are not unique to unbalanced sets, do not account for true negatives (TN), and are calculated for individual classes, the Matthews correlation coefficient (MCC) expressed by equation (8) [20,21,23] will also be calculated. This coefficient takes into account the TP , TN , FP , and FN scores, and does not favor a dominant class, which translates into robustness to an unbalanced dataset. This coefficient always has a maximum value of 1, while the minimum value depends on the number and distribution of classes – this means that the minimum value will range from -1 to 0.

$$MCC = \frac{c \cdot s - \sum_k^K p_k \cdot t_k}{\sqrt{(s^2 - \sum_k^K p_k^2) \cdot (s^2 - \sum_k^K t_k^2)}} \quad (8)$$

where: c – total number of samples correctly classified, s – total number of classifications, p_k – number of times class k has been predicted, t_k – number of times class k actually occurred.

4. RESULTS

Four classification algorithms were used to process the collected data: k-NN, SVM (SVC - Support Vector Classifier), Random Forest, and MLP neural network. Each model was trained using training data collected offline. For each model, it was necessary to select model hyperparameters. The hyperparameters were selected using a grid search method, which involves examining all combinations according to a predefined list of parameter variants [24]. The models were implemented in Python using the scikit-learn package.

In the case of the SVM and Random Forest classifiers, due to their sensitivity to unbalanced training data sets, a weight correction was applied, expressed by equation (9) [25,26].

$$Class_{weight} = \frac{samples_{num}}{class_{count} \cdot class_{freq}} \quad (9)$$

where: $Class_{weight}$ – class weight, $samples_{num}$ – the number of all class elements, $class_{count}$ – number of all classes, $class_{freq}$ – class frequency.

This correction is inversely proportional to the frequency of occurrence of a given class in the training data set [27,28].

4.1. k-NN

The following hyperparameters were selected for the k-NN model [29]:

- weights = 'uniform' – weight function used during prediction, all points are treated equally,
- neighbors = 15 – number of neighbors taken into account,
- algorithm = 'auto' – automatic selection of the algorithm for searching for nearest neighbors.

Tab. 4. Metrics of individual classes for the k-NN model

Class	Recall	Precision	F_1
'East'	0.46	0.41	0.43
'North'	0.34	0.43	0.38
'South'	0.13	0.33	0.19
'West'	0.64	0.50	0.56

Table 4 presents the precision, sensitivity, and F_1 score for each k-NN class. The best-detected direction was west, containing 39 samples, representing 35.1% of the test set. It achieved the highest sensitivity of 0.64, meaning that 64% of the true west orientations were correctly identified. A precision of 50% means that half of the cases were false positives. The F_1 score indicates that the relationship between sensitivity and precision is balanced.

The south class achieved the worst result, achieving a sensitivity of 13%. This class contained 15 samples, representing 13.5% of the test set. Precision, on the other hand, was 33%.

The north and east directions achieved moderate performance, with the east direction achieving slightly better results.

Tab. 5. Metrics for the k-NN model

Precision macro	Recall macro	F_1 macro	Micro score	MCC
0.42	0.40	0.39	0.45	0.23

Table 5 presents the global metrics of the classifier. All macro-averages and micro-averages indicate moderate classifier performance. The classifier achieved an accuracy (micro score) of 0.45. The MCC coefficient reached a value of 0.23, indicating poor classifier performance.

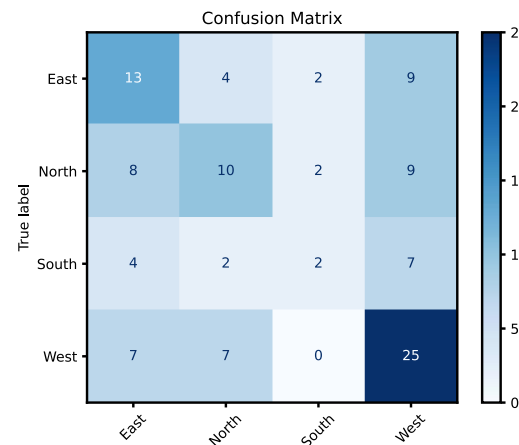


Fig. 10. Confusion matrix for the k-NN model

The confusion matrix presented in Figure 10 shows that all directions are most frequently confused with west. East and north were each classified as west nine times, while south was classified as west seven times. An asymmetry in errors between south and west is visible. South was classified as west seven times, while west was never classified as south.

4.2. SVM

Class corrections were applied to the SVM (SVC) model as described in section 4. The selected hyperparameters were [27]:

- Kernel = 'poly' – type of kernel used for calculations,
- Regularization = 10 – the value of parameter C affecting the objective function, it limits overfitting,
- Gamma = 1 – kernel function factor,
- Degree = 4 – degree of the polynomial of the 'poly' kernel.

Tab. 6. Metrics of individual classes for the SVC model

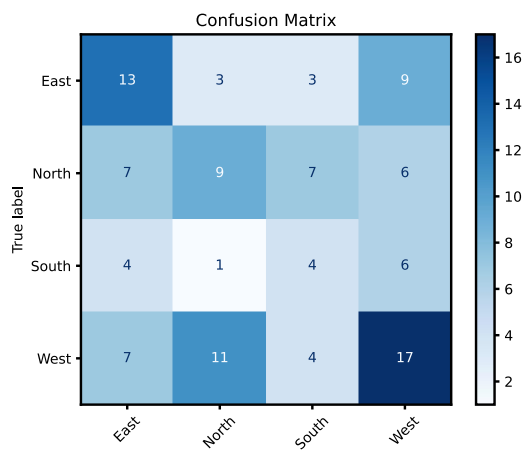
Class	Recall	Precision	F_1
'East'	0.46	0.42	0.44
'North'	0.31	0.38	0.34
'South'	0.27	0.22	0.24
'West'	0.44	0.45	0.44

Table 6 presents the metric results for the SVC model. The classifier best classified the west and east directions. Both classes achieved the F_1 score of 0.44. The east direction achieved a sensitivity of 0.46, meaning that 46% of actual cases for this orientation were correctly classified. For the west direction, this was 44%. Precision was also similar in both cases, reaching 0.42 for the east direction and 0.45 for the west direction, respectively. This means that in over 50% of cases, these directions were incorrectly classified. The south direction achieved the worst performance. Sensitivity was 0.27 and precision 0.22. For the north direction, sensitivity was 0.31 and precision 0.38.

Tab. 7. Metrics for the SVC model

Precision macro	Recall macro	F_1 macro	Micro score	MCC
0.37	0.37	0.37	0.39	0.16

Table 7 presents the global metrics of the classifier. All macro-averages and micro-averages indicate moderate performance of the classifier. The classifier achieved an accuracy of 0.39. Despite the moderate metric values, the MCC coefficient reaches a value of 0.16, indicating poor performance of the classifier.

**Fig. 11.** Confusion matrix for the SVC model

Analyzing the confusion matrix in Figure 11 demonstrates that the east and south directions were most frequently misclassified as west. In the north direction, the errors were evenly distributed among the classes. The direction of the west was most frequently misclassified as north.

4.3. Random Forest

Similarly to the SVM model, weight correction was applied. The model parameters were determined as follows [28]:

- max_depth = None – maximum tree depth, none means no

limit,

- min_samples_leaf = 4 – minimum required number of samples to constitute a leaf node,
- min_samples_split = 10 – minimum number of samples required to split an internal node,
- n_estimators = 50 – number of trees in the forest.

Due to the operation of the algorithm, in order to achieve deterministic behavior of the model, the seed in a random number generator was also selected and was set to 3013327208.

Tab. 8. Class metrics for Random Forest Classifier

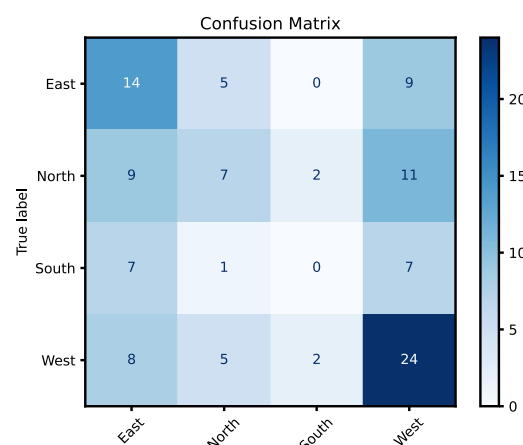
Class	Recall	Precision	F_1
'East'	0.50	0.37	0.42
'North'	0.24	0.39	0.30
'South'	0.00	0.00	0.00
'West'	0.62	0.47	0.53

Table 8 presents the metrics for the Random Forest model. The west direction had the best sensitivity of 0.62. This means that 62% of actual cases of this orientation were correctly classified. More than 50% of cases classified as west were incorrect, with precision of 0.47. The east direction is distinguished by a precision of 0.37 and a sensitivity of 0.50, resulting in the F_1 score of 0.42. This indicates moderate performance for this class. Sensitivity was inferior to precision in the north class. The south class received zero results, indicating that it was never properly identified.

Tab. 9. Class metrics for Random Forest Classifier

Precision macro	Recall macro	F_1 macro	Micro score	MCC
0.31	0.34	0.31	0.41	0.16

The global metrics presented in Table 9 show moderate classifier performance. The low MCC value of 0.16 indicates poor classifier performance.

**Fig. 12.** Confusion matrix for the Random Forest model

The confusion matrix (Figure 12) indicates that the most frequently confused directions were west and east. South was not correctly classified even once. There is a visible asymmetry in errors between the south and other classes. South was classified as east 7 times, east as south 0 times, south was classified as west 7

times, and west as south 2 times.

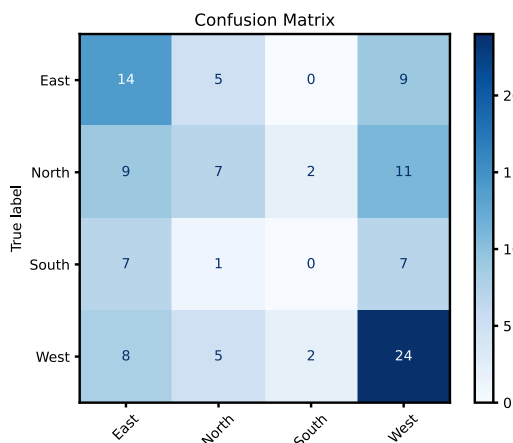


Fig. 12. Confusion matrix for the Random Forest model

4.4. MLP Classifier

The hyperparameters of the MLP classifier were determined as follows [30]:

- solver = 'adam' – optimizer,
- activation = 'relu' – activation function,
- hidden_layers_size = (150, 75) – structure of the neural network,
- max_iter = 50000 – maximum number of epochs.

Again, due to the operation of the algorithm, in order to achieve deterministic behavior of the model, the seed in a random number generator was also selected and was set to 496680515.

Tab. 10. Class metrics for MLP Classifier

Class	Recall	Precision	F_1
'East'	0.54	0.39	0.45
'North'	0.34	0.40	0.37
'South'	0.13	0.20	0.16
'West'	0.46	0.47	0.47

Table 10 demonstrates the MLP classifier metrics. The highest sensitivity was achieved for the east direction, at 0.54. This means that 54% of actual cases for this orientation were correctly classified. The precision for the east direction was 0.38, resulting in a combined F_1 score of 0.45. The west direction achieved a sensitivity of 0.46 and a precision of 0.47, resulting in the F_1 score of 0.47, thus better than the east direction. The south direction achieved the worst metrics, with a sensitivity of 13%, a precision of 0.20, and the F_1 score of 0.16. The north direction had a sensitivity of 0.34, a precision of 0.40, and a combined F_1 score of 0.37.

Tab. 11. Class metrics for MLP Classifier

Precision macro	Recall macro	F_1 macro	Micro score	MCC
0.37	0.37	0.36	0.41	0.18

The overall model metrics are presented in Table 11. The macro-average sensitivity and precision were 0.37, and the F_1 score was 0.36. These results indicate moderate classifier perfor-

mance. A low MCC value indicates overall poor classifier performance.

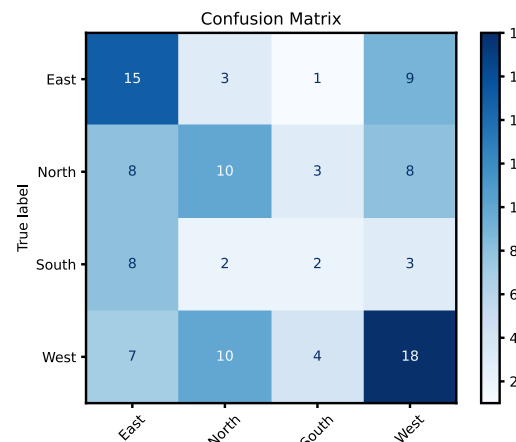


Fig. 13. Confusion matrix for the MLP Classifier model

The confusion matrix of the MLP classifier shown in Figure 13 indicates that the most frequently confused directions were east and west. The south direction was correctly classified in two cases, most often as east. The north direction was classified eight times each as west and east.

4.5. Results discussion

The k-NN model achieved the highest values for all metrics. The MLP and SVM models performed similarly, with the MLP classifier marginally better in terms of micro-averages and the MCC coefficient. The SVM classifier's metrics are balanced. Although the Random Forest classifier generally performs worse than the other classifiers, its micro-score is comparable to that of the MLP neural network due to its high sensitivity to the west direction. This model's metrics are underestimated due to the classifier's zero performance in the south direction.

The east, north, and south directions are classified as west by all models, which is consistent with the predominant position of this class in the training dataset, as illustrated in Table 2. Subsequently, each classifier achieved the most favorable metrics in the west direction. SVC is an exception, achieving the F_1 score of 0.44 in both the east and west directions.

The west direction is evidently favored by the k-NN and Random Forest classifiers. This corresponds to a good F_1 score of 0.56 for k-NN and 0.53 for Random Forest.

The asymmetries in the error distributions are most noticeable in the south direction. Among other factors, this is attributable to the imbalance of the training set and the limited number of samples from this direction in the test set (13.5% of the set size).

The poor performance of the classifiers in relation to the South class is due to the imbalance of the training set, even though the imbalance is compensated by weight correction in the case of the SVM and Random Forest classifiers.

5. FURTHER RESEARCH

Further research is planned to enhance the quality of estimation by expanding the switchable multi-antenna system. The implemented dual-antenna switched array is characterized by simple de-

sign, low cost, and easy scalability. Increasing the number of antennas enables greater exploitation of spatial diversity through information multiplication, while avoiding unnecessary system complexity or cost increases in implementation.

To fully utilize the benefits resulting from the switchable multi-antenna array, work will also be conducted on increasing the sampling frequency of signal measurements. Furthermore, increased sampling will enable effective estimation of the orientation of a moving object. This is intended to be achieved through the use of newer Wi-Fi standards and a redesign of the measurement infrastructure. Preliminary simulation studies have shown that sampling of 15 samples per location allows for a reduction of MAE value by more than a factor of 3 [31].

Tab. 12. Sample results of localization based on dual antenna RSSI readouts

Classifier	MAE [m]	RMSE [m]	Stdev [m]
k-NN	1.53	1.90	1.30
MLP Classifier	1.46	1.82	1.06
Random Forest	1.63	1.94	1.35
SVM Classifier	1.54	1.90	1.25

Tab. 13. Sample results of localization based on single antenna RSSI readouts

Classifier	MAE [m]	RMSE [m]	Stdev [m]
k-NN	1.61	2.00	1.38
MLP Classifier	1.64	1.99	1.10
Random Forest	1.65	1.97	1.47
SVM Classifier	1.55	1.98	1.43

The results presented in Table 12 show exemplary results of location estimation based on RSSI measurements using selected classifiers. For each classifier, mean absolute errors (MAE), root mean square errors (RMSE), and standard deviations (Stdev) were calculated. Analysis of the results shows that it is possible to achieve MAE at the level of even 1.46 m, RMSE of 1.82 m and Stdev of 1.06 m when using an MLP network. This means that location estimation with moderate accuracy is possible, which can be applied in sector-based localization. The values presented in the table are slightly higher than similar studies performed in publications [32] (MAE \approx 0.50 m, RMSE \approx 0.76 m) and [33] (RMSE \approx 0.247 m). In well-controlled indoor environments (good anchor geometry, minimal multipath/obstruction) error on the order of 0.2 – 1 m is possible. In more realistic or cluttered indoor environments, errors of a few metres (2–4 m) are common.

The results presented in Table 13 show the outcomes obtained for estimation with the use of a single antenna. It is evident that the application of data from both antennas results in improved results in all considered cases. For the MLP Classifier, a MAE difference of 0.18 m, RMS of 0.17 m, and a Stdev reduction of 0.04 m were obtained.

Further work anticipates a comprehensive estimation of both orientation and location of the tracked object based on received signal strength measurements.

6. CONCLUSIONS

The outcomes of experimental research on a mobile robot's orientation estimation are presented in this article. The objective of

the investigation was to evaluate the feasibility of determining orientation in relation to the cardinal directions (N, W, S, E) by analyzing the difference in RSSI values in a dual-antenna tracker that employs the Wi-Fi standard and machine learning fingerprinting techniques.

The results of the studies that have been presented indicate that it is feasible to determine orientation and location with moderate precision. The results obtained are significantly influenced by the imbalance of the training set, which results in differentiating the performance of the model among individual classes. The quality of the developed models can be enhanced by giving training data collection extra attention to guarantee that the final set is as balanced as possible.

Simulation studies [31] have shown that the performance of classifiers can be enhanced by increasing the number of signal samples measured at a specific location. However, this is constrained by the speed of RSSI measurement and the number of hardware resources available. Furthermore, this approach has the potential to mitigate the effects of interfering phenomena.

Further research is planned to enhance the quality of estimation and facilitate dynamic object tracking by expanding the switchable multi-antenna system and implementing the most recent Wi-Fi standards. The use of a multi-antenna switchable array allows maintaining low implementation cost and maximizing the benefits of antenna spatial diversity – more antennas enable obtaining more data correlated with orientation and location.

REFERENCES

1. Leitch SG, Ahmed QZ, Abbas WB, Hafeez M, Laziridis PI, Sureephong P et al. On Indoor Localization Using WiFi, BLE, UWB, and IMU Technologies. *Sensors*. 2023;23(20):8598.
2. Wang R, Niu G, Cao Q, Chen CS, Ho SW. A Survey of Visible-Light-Communication-Based Indoor Positioning Systems. *Sensors*. 2024;24(16):5197.
3. Hailu TG, Guo X, Si H, Li L, Zhang Y. Theories and Methods for Indoor Positioning Systems: A Comparative Analysis, Challenges, and Prospective Measures. *Sensors*. 2024;24(21):6876.
4. Zafari F, Gkelias A, Leung KK. A Survey of Indoor Localization Systems and Technologies. *IEEE Commun Surv Tutor*. 2019;21(3): 2568–99.
5. Yang T, Cabani A, Chafouk H. A Survey of Recent Indoor Localization Scenarios and Methodologies. *Sensors*. 2021;21(23):8086.
6. Brena RF, García-Vázquez JP, Galván-Tejada CE, Muñoz-Rodríguez D, Vargas-Rosales C, Fangmeyer J. Evolution of Indoor Positioning Technologies: A Survey. *J Sens*. 2017;1–21.
7. Santoro L, Nardello M, Brunelli D, Fontanelli D. UWB-Based Indoor Positioning System With Infinite Scalability. *IEEE Transactions on Instrumentation and Measurement*. 2023;72:1–11.
8. Li P, Wu W, Zhao Z, Huang GQ. Indoor positioning systems in industry 4.0 applications: Current status, opportunities and future trends. *Digit Eng*. 2024;3:100020.
9. Ouyang G, Abed-Meraim K. A Survey of Magnetic-Field-Based Indoor Localization. *Electronics*. 2022;11(6):864.
10. Guan J, Chen Z, Jiang G. Research on Calibration Method of Triaxial Magnetometer Based on Improved PSO-Ellipsoid Fitting Algorithm. *Electronics*. 2025;14(9):1778.
11. Bluetooth® Technology Website [Internet]. 2025 [cited 2025 July 16]. Direction Finding. <https://www.bluetooth.com/learn-about-bluetooth/feature-enhancements/direction-finding/>
12. Wielandt S, Strycker L. Indoor Multipath Assisted Angle of Arrival Localization. *Sensors*. 2017;17(11):2522.

13. Ciężkowski M, Kociszewski R. Fast 50 Hz Updated Static Infrared Positioning System Based on Triangulation Method. *Sensors*. 2024;24(5):1389.
14. Malajner M, Planinsic P, Gleich D. Angle of Arrival Estimation Using RSSI and Omnidirectional Rotatable Antennas. *IEEE Sens J*. 2012;12(6):1950–7.
15. Burton T, Rasmussen K. Orientation Estimation using Wireless Device Radiation Patterns [Internet]. arXiv; 2022 [cited 2025 July 17]. <http://arxiv.org/abs/2203.10052>
16. esp32-wroom-da_datasheet_en.pdf [Internet]. [cited 2025 July 16]. https://www.espressif.com/sites/default/files/documentation/esp32-wroom-da_datasheet_en.pdf
17. BNO080_085-Datasheet.pdf [Internet]. [cited 2025 July 16]. https://www.ceva-ip.com/wp-content/uploads/BNO080_085-Datasheet.pdf
18. DJI [Internet]. [cited 2025 July 16]. Support for RoboMaster S1. <https://www.dji.com/pl/support/product/photo>
19. Aguilar-Ruiz JS, Michalak M. Classification performance assessment for imbalanced multiclass data. *Scientific Reports*. 2024 May 10;14(1).
20. Grandini M, Bagli E, Visani G. Metrics for Multi-Class Classification: an Overview [Internet]. arXiv; 2020 [cited 2025 July 17]. <http://arxiv.org/abs/2008.05756>
21. Chicco D, Jurman G. The advantages of the Matthews correlation coefficient (MCC) over F1 score and accuracy in binary classification evaluation. *BMC Genomics*. 2020;21(1).
22. scikit-learn [Internet]. [cited 2025 July 17]. 3.4. Metrics and scoring: quantifying the quality of predictions. https://scikit-learn/stable/modules/model_evaluation.html
23. Chicco D, Jurman G. The Matthews correlation coefficient (MCC) should replace the ROC AUC as the standard metric for assessing binary classification. *BioData Mining*. 2023;16(1).
24. Subaşı N. Comprehensive Analysis of Grid and Randomized Search on Dataset Performance. *Eur J Eng Appl Sci*. 2024;7(2):77–83.
25. Hasib KMd, Iqbal MdS, Shah FM, Al Mahmud J, Popel MH, Showrov MdIH et al. A Survey of Methods for Managing the Classification and Solution of Data Imbalance Problem. *J Comput Sci*. 2020;16(11):1546–57.
26. Chen C, Breiman L. Using Random Forest to Learn Imbalanced Data. University of California, Berkeley. 2004. <https://statistics.berkeley.edu/tech-reports/666>
27. scikit-learn [Internet]. [cited 2025 July 18]. SVC. <https://scikit-learn/stable/modules/generated/sklearn.svm.SVC.html>
28. scikit-learn [Internet]. [cited 2025 July 18]. RandomForestClassifier. <https://scikit-learn/stable/modules/generated/sklearn.ensemble.RandomForestClassifier.html>
29. scikit-learn [Internet]. [cited 2025 July 18]. KNeighborsClassifier. Available from: <https://scikit-learn/stable/modules/generated/sklearn.neighbors.KNeighborsClassifier.html>
30. scikit-learn [Internet]. [cited 2025 July 23]. MLPClassifier. https://scikit-learn/stable/modules/generated/sklearn.neural_network.MLPClassifier.html
31. Sumorek M, Idźkowski A. The influence of recursive filtering methods on Bluetooth-based localization. *IFAC-Pap*. 2024;58(9):126–31.
32. Antonopoulos K, Skandamis T, Alogdianakis G, Faliagka E, Antonopoulos CP, Voros N. Indoor Localization and ADL Monitoring via RSSI-Driven ML with Feedback Process. *Electronics*. 2025;14(19):3759. <https://doi.org/10.3390/electronics14193759>
33. Sahnoun S, Souissi R, Chiboub S, Chabchoub A, Baazaoui MK, Fakhfakh A, Derbel F. Enhancing Localization Accuracy and Reducing Processing Time in Indoor Positioning Systems: A Comparative Analysis of AI Models. *Sensors*. 2025; 25(2):475. <https://doi.org/10.3390/s25020475>

The research was carried out as part of work no. WI/WE-IA/6/2024 at the Bialystok University of Technology and financed by a research subsidy provided by Ministry of Science and Higher Education.

Mateusz Sumorek:  <https://orcid.org/0009-0003-2440-9556>

Adam Idźkowski:  <https://orcid.org/0000-0002-1671-8979>



This work is licensed under the Creative Commons BY-NC-ND 4.0 license.